

See discussions, stats, and author profiles for this publication at: <https://www.researchgate.net/publication/281971747>

Dipole Moment Effect of Cyano-Substituted Spirofluorenes on Charge Storage for Organic Transistor Memory

ARTICLE in THE JOURNAL OF PHYSICAL CHEMISTRY C · JULY 2015

Impact Factor: 4.77 · DOI: 10.1021/acs.jpcc.5b03867

READS

57

10 AUTHORS, INCLUDING:



Ling-Hai Xie

Nanjing University of Posts and Telecommuni...

149 PUBLICATIONS 1,983 CITATIONS

[SEE PROFILE](#)



Ling Haifeng

Nanjing University of Posts and Telecommuni...

8 PUBLICATIONS 39 CITATIONS

[SEE PROFILE](#)



Jin Wang

Nanjing University of Posts and Telecommuni...

5 PUBLICATIONS 1 CITATION

[SEE PROFILE](#)



Wei Huang

University of Hawai'i at Mānoa

1,354 PUBLICATIONS 30,854 CITATIONS

[SEE PROFILE](#)

Dipole Moment Effect of Cyano-Substituted Spirofluorenes on Charge Storage for Organic Transistor Memory

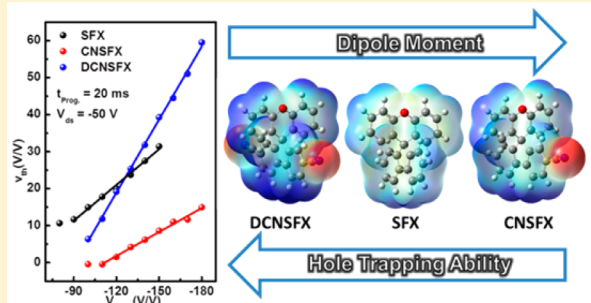
Chen Sun,[†] Zongqiong Lin,[†] Wenjuan Xu,[†] Linghai Xie,^{*,†} Haifeng Ling,[†] Mingyang Chen,[†] Jin Wang,[†] Ying Wei,[†] Mingdong Yi,^{*,†} and Wei Huang^{*,†,‡}

[†]Key Laboratory for Organic Electronics and Information Displays & Institute of Advanced Materials(IAM), Jiangsu National Synergetic Innovation Center for Advanced Materials (SICAM), Nanjing University of Posts & Telecommunications, 9 Wenyuan Road, Nanjing 210023, China

[‡]Key Laboratory of Flexible Electronics (KLOFE) & Institute of Advanced Materials (IAM), Jiangsu National Synergetic Innovation Center for Advanced Materials (SICAM), Nanjing Tech University (NanjingTech), 30 South Puzhu Road, Nanjing 211816, China

S Supporting Information

ABSTRACT: As a fascinating information storage device, organic transistor memory based on molecular charge storage elements (MCSEs) has attracted great research interest. However, the charge storage mechanism of MCSEs is ambiguous due to their complex charge dynamic behaviors. Herein, the dipole moment effects on the charge trapping process and the performance of transistor memory are revealed based on cruciform spiro[fluorene-9,9'-xanthene] (SFXs), incorporating cyano moieties, as the typical electron-withdrawing substitution. The characterization of electrostatic potential (ESP) calculation, UV-vis, photoluminescence, and crystallography of SFXs shows the SFXs MCSEs with weaker dipole moment through symmetrical substitution. A series of prototype transistor memories based on SFXs exhibit an erasable type feature with smart photoresponsive behavior. The weaker dipole moment ones possess larger memory window (~ 40 V), higher charge trapping density ($> 1 \times 10^{13} \text{ cm}^{-2}$), and higher programming speed ($10^{14}\text{--}10^{11} \text{ cm}^{-2} \text{ s}^{-1}$). The hole trapping process is dominated by the dipole moment rather than the charge dissipation when compared with different SFXs at the same HOMO level. Rather good charge retention property ($> 10^4$ s) and large on/off ratio ($\sim 10^4$) are obtained by blending SFXs with polymer dielectrics in optimized devices. The dipole moment effects on the charge trapping behavior provide not only the design of high performance transistor memory but also the smart information encryption in future data storage.



INTRODUCTION

Organic memory devices have attracted extensive attention for the future information storage toward the era of big data and flexible electronics on account of their good scalability, light weight, and low-cost fabrication process.^{1–4} The nonvolatile organic field-effect transistor (OFET) memory is one of the most striking devices with nondestructive read-out and multibit storage property, whose conductivity can be easily manipulated by tuning the charge behavior between the channels.^{5–7} Furthermore, the open channel of FET configuration facilitates the charge tuning through the external stimulation such as light irradiation and gas or biomaterial exposure, leading to remarkable smart responsive behavior.^{8–11} The thorny challenge in OFET memory is the design of trapping element and getting deep insight into the trapping mechanism with high density and long-term charge maintenance.

The molecular charge storage elements (MCSEs) have great superiority in charge density over the well-investigated nanofloating gate^{12–15} with a designable molecular structure, flexible synthesis, and tunable bandgap.^{16,17} However, the memory performance is dominated not only by the F–N

(Fowler–Nordheim) tunneling barrier between the transport layer and MCSEs but also by several other factors.^{18–20} Because of the polymorphic behavior in the condensed state, the polymer-based MCSEs are ambiguous in charge trapping mechanism; meanwhile, they have several drawbacks such as multistep synthesis and uncontrollable molecular weight.^{21–23} Therefore, using small-molecule compounds as MCSEs is a promising way to realize the high-density information storage with reliable charge maintenance in transistor memory and further clarify the charge trapping mechanism.^{24,25} Although the investigation in the correlation between charge storage behavior and small molecular MCSEs is limited,^{26–28} there are still some useful results that enlighten us with the design of MCSEs materials, especially from the polymer dielectrics. Kim's group concluded that the hydrophobic and nonpolar polymers displayed a larger amount of charge storage than that of hydrophilic and polar polymers owing to the rapid dissipation

Received: April 22, 2015

Revised: July 1, 2015

Published: July 15, 2015



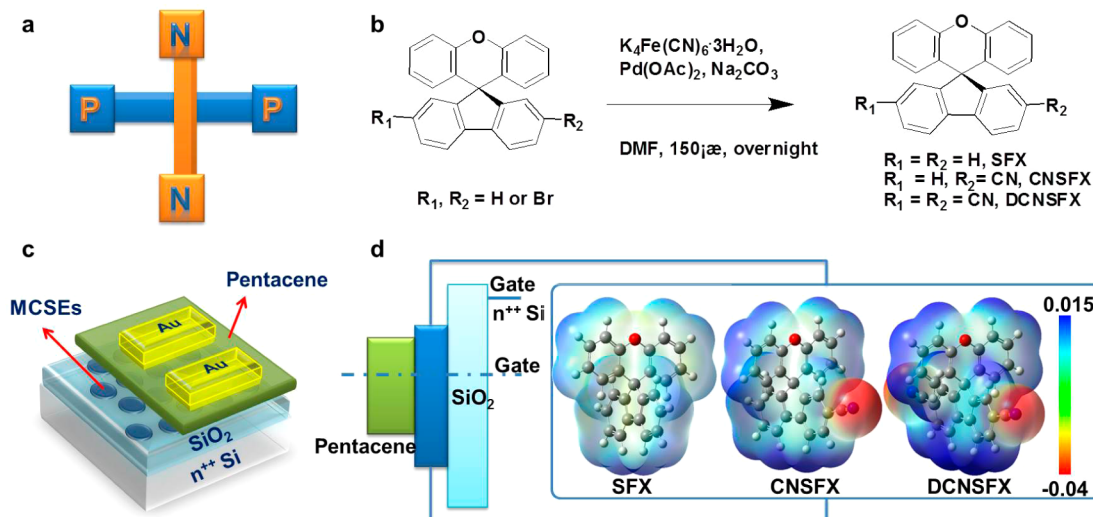


Figure 1. (a) Design of the organic charge trapping elements (MCSEs) toward transistors memory. (b) Synthetic procedures for the CNSFX and DCNSFX. (c) Schematic configuration of the transistor memory device. (d) Energy level diagrams and electrostatic potential (ESP) of the SFXs (calculated by density functional theory calculations).

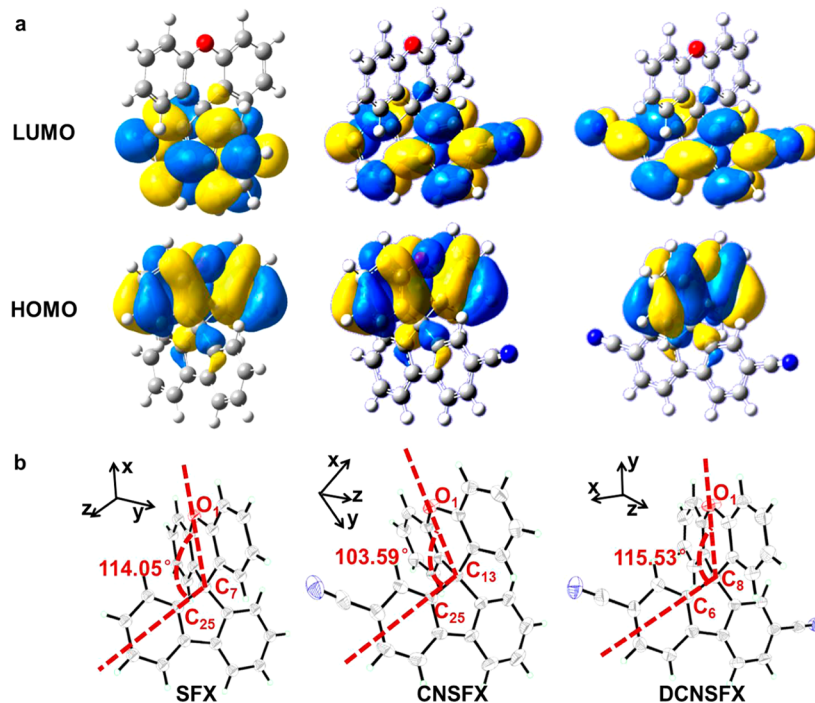


Figure 2. (a) HOMO and LUMO calculated using the B3LYP/6-31G basis set. (b) Crystal structure and the dihedral angles of SFX, CNSFX, and DCNSFX.

of transferred charges leading to a smaller polarity.²⁹ According to previous studies, a larger interface interfacial dipole dominated by the dipole moment of organic species³⁰ can result in a significant charge transfer behavior,³¹ which plays a vital role in the dynamic behavior of charge injection, storage, and delivery in transistor memory. We believe that the intrinsic dipole moment of a small molecule, rather than the charge dissipation, may play a vital role in the charge transfer between the MCSEs and the transport layer at the interface of their heterojunction as a result of the variety of memory performance.

According to previous researches, topological structure and nonplanar conformations of star-shaped polymers will generate

more charge trapped centers to help enlarge the superior charge-trapping capability.^{32–34} Furthermore, the steric hindrance effect coming from a large dihedral angle of electron donor–spacer–acceptor push–pull organic small molecules (PPOMs) benefits the charge trapping at the nanointerface of heterojunction according to Lee et al.¹⁸ As a typical nonplanar organic semiconductor, the cruciform spiroarene with a typical supramolecular steric hindrance is one of the most promising MCSEs for high performance transistor memory.³⁵ The dipole moment effects of spiroarene MCSEs can be well investigated to get rid of their energy level effect due to the separation of highest occupied molecular orbital (HOMO) and lowest unoccupied molecular orbital (LUMO) level which makes it

possible to tune their dipole moment independently. Furthermore, such separation of HOMO and LUMO offers a rather good photoresponse according to their phototransistor results.³⁶ Herein, we successfully adjust the dipole moment of MCSEs based on a p–n type cruciform spiro[fluorene-9,9'-xanthene] (SFX) through different cyano substitution (Figure 1a,b) to investigate the dipole moment effects on the charge trapping behavior in transistor memory (Figure 1c).

RESULTS AND DISCUSSION

Synthesis and Dipole Moment of Cyano-Substituted SFXs. The cyano-substituted SFXs in different dipole moment are synthesized without changing their HOMO level, where the p- and n-type moieties are separated vertically from each other. Figure 1b shows the synthetic route and structure of SFX, CNSFX, and DCNSFX. The substrate SFX derivatives are prepared by the unexpected one-pot method which we had explored in our previous work,^{37,38} and the cyano-substituted SFX derivatives are obtained according to previously reported cyanozation methods.³⁹ Subsequently, the electron-withdrawing cyano group efficiently reacted with the derivatives of SFXs to give the target compounds CNSFX and DCNSFX with yields of 85% and 75%, respectively. The detailed synthesis and chemical structures of final products are confirmed with ¹H NMR spectroscopy, GC-MS spectroscopy, and elemental analysis (Figures S1 and S2) and found to be in good agreement with the structure.

Electrostatic potentials (ESP) of SFXs are calculated to investigate the relationship between the essential charge dispersion and dipole moment. According to the charge density distribution analysis of ESP (Figure 1d), we find that charges are evenly distributed on SFX without any supramolecular functionalization. However, owing to the electron-withdrawing cyano moiety in CNSFX, the charge density distribution changes dramatically as the electrons located at the nitrogen atom. Therefore, charges are mainly asymmetrical localized on the cyano group side of CNSFX with the charge distribution point to the opposite side, leading to a strong dipole moment. Similarly, the electrons in DCNSFX mainly accumulate on the cyano groups of fluorene moiety, which means nearly the same charge dispersion as that of CNSFX. But the symmetrical charge distribution of DCNSFX eventually reaches the equilibrium state as a result of a weak dipole moment finally.

The theory calculation of cyano-substituted SFXs is performed by Gaussian 09 with the method of density functional theory (DFT)/B3LYP/6-31G with separated HOMO and LUMO levels. The energy diagram of SFXs is shown in Figure 2a. All these three MCSEs exhibit nearly the same HOMO level (~−5.89 eV), whose electronic wave functions are located at the xanthene plane, while the wave function at the cyano-substituted fluorene plane contributes to the LUMO level. The cyano substitutions only decrease their LUMO level to −0.86, −1.73, and −2.36 eV for SFX, CNSFX, and DCNSFX, respectively. Introducing the electron-withdrawing cyano groups into SFXs effectively decreases their LUMO levels without changing the HOMO levels or the hole tunneling barrier of pentacene/SFXs (~0.99 eV). Therefore, the dipole moment effects of SFXs on the hole trapping can be well investigated to exclude the influence of their energy levels. Cyclic voltammetry (CV) (Figure S3) further indicates similar results. The HOMOs of SFX, CNSFX, and DCNSFX energy levels are −6.11, −6.12, and −6.17 eV and LUMOs are −1.88,

−2.41, and −2.79 eV, respectively. We extract the dipole moment of SFXs from their energy level calculation and list the results in Table 1. As expected, the total dipole moment can be

Table 1. Comparison of the Dipole Moments (in D) of SFX, CNSFX, and DCNSFX

	X	Y	Z	total
SFX	−0.9763	0.0140	−0.1946	0.9956
CNSFX	3.0081	4.5857	−0.5415	5.5110
DCNSFX	−0.2041	−1.5794	0.0052	1.5925

ordered as μ_{SFX} (0.9956 D) < μ_{DCNSFX} (1.5925 D) ≪ μ_{CNSFX} (5.5110 D). The dipole moment of CNSFX mainly directs to the y-axis, opposite to the cyano group. In order to get insight into the cruciform configuration and the steric hindrance of SFXs, the single crystal of CNSFX and DCNSFX is cultivated for analysis (SFX data coming from the CCDC database). The crystal structures are displayed in Figure 2b, and the CCDC reference numbers of CNSFX and DCNSFX are 1035980 and 1035982, respectively. According to the analysis of X-ray crystallography, we find that SFXs possess nonplanar cross-link conformation. However, the dihedral angle between fluorene and xanthene are not strictly vertical to each other due to the remarkable steric hindrance in SFXs. The dihedral angles of SFXs are measured with 114.05° ($\angle \text{O}_1\text{C}_7\text{C}_{25}$), 103.59° ($\angle \text{O}_1\text{C}_{13}\text{C}_{25}$), and 115.53° ($\angle \text{O}_1\text{C}_8\text{C}_6$) for SFX, CNSFX, and DCNSFX, respectively, which are smaller than the ideal angle of ~120°. More importantly, the CNSFX exhibits the smallest dihedral angle, where the xanthene bends toward the cyano moiety due to its strong electron withdrawing, and the balance comes back in the case of DCNSFX, with two symmetrical cyano groups at the fluorene moiety. The steric hindrance may generate more charge trapping sites to improve their memory performances.^{32,33} The monocyano-substituted CNSFX will behave a rather strong dipole moment and provide further comparison of device performance.

Fabrication of SFXs Film for Transistor Memory. The SFXs-based MCSEs films are fabricated by thermal evaporation as described in the experimental part. The UV-vis absorption and photoluminescence (PL) analysis of SFX, CNSFX, and DCNSFX films are measured to further illustrate the dipole moment effects on the optical property in aggregation compared with that in diluted dichloromethane solutions (Figures S4 and S5). All these three films of SFXs suffer a slight red-shift (~10 nm) in UV-vis profiles due to the aggregation as in most organic semiconductor films. These strong intermolecular aggregations would be useful to afford more trapped charges of transistor memory devices. The change of SFX film's PL profile ~325 nm may be ascribed to the self-absorption in the film (the ~450 emission band coming from the excimer). However, as the strong total dipole moment of CNSFX, the emission peak of its film shows a remarkable red-shift from 340 to 382 nm. The DCNSFX film even exhibits a slight blue-shift in PL, indicating a much weaker dipole moment.

Figure 3a–c shows the atomic force microscopy (AFM) images of the deposited SFXs films (~5 nm thick) under vacuum on bare SiO₂ substrates. The MCSEs film exhibits a surface morphology with separated islands, which is favorable for the long-term charge storage, according to previous studies.⁴⁰ AFM images of pentacene on top of SFXs film are shown in Figure 3d–f. The pentacene/DCNSFX exhibits a

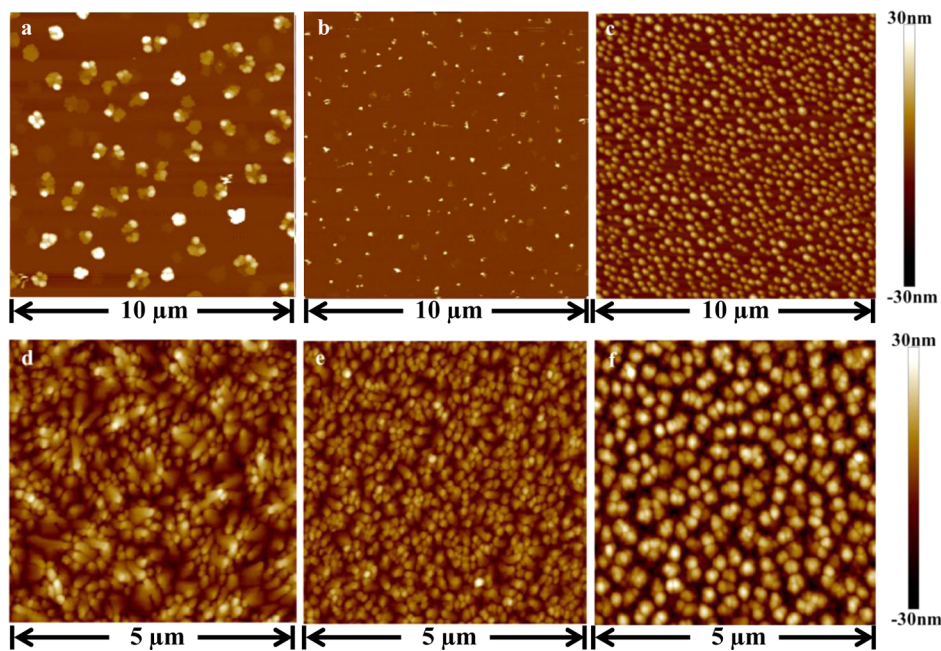


Figure 3. (a–c) AFM topographic images of SFX (a), CNSFX (b), and DCNSFX (c) films on SiO₂/Si substrates. (d–f) AFM topographic images of pentacene on different surfaces: (d) SFX, (e) CNSFX, and (f) DCNSFX modified SiO₂ surface.

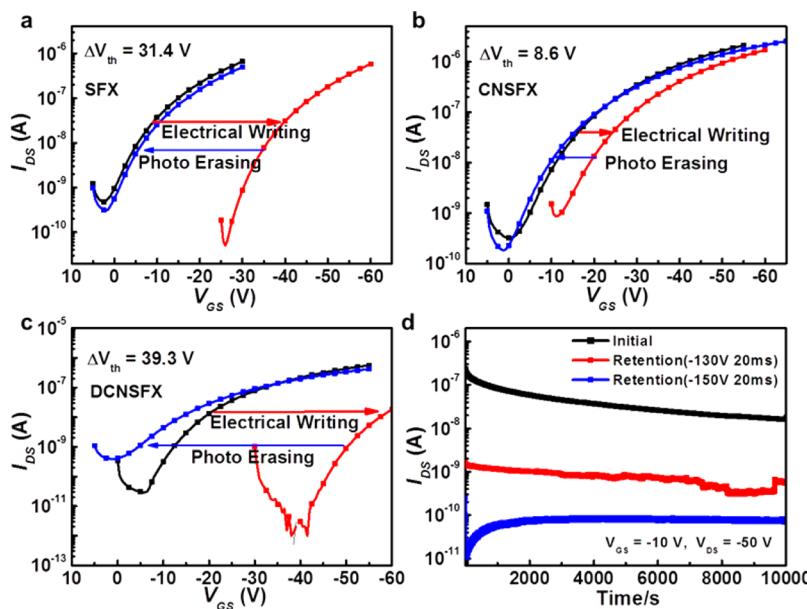


Figure 4. (a–c) Reversible shifts in V_{th} and the transfer characteristics of the transistors before and after gate bias in dark with SFXs as MCSEs. The drain current was measured at $V_{ds} = -50$ V. The programming bias (V_{Prog}) is -160 V, and programming time (t_{Prog}) is 20 ms. (d) Retention test of multibit storage with three levels for DCNSFX-based transistor.

remarkably smaller grain domain with the size of approximately 0.2–0.3 μm than the growth layer of pentacene in a standard transistor, even larger than that of pentacene/CNSFX. It may be ascribed to the rough dielectric surface which impedes the lateral pentacene molecular diffusion and suppresses the ordered pentacene molecular nucleation, as a result of the degeneration of device mobility. Then, we deposit Au on pentacene film to construct a typical p-type transistor. Figure 1c presents the schematic diagrams of prototype pentacene-based transistor memories based on a bottom-gate top-contact configuration in which SFX, CNSFX, and DCNSFX are used

as the MCSEs between pentacene and dielectric layer to investigate their trapping abilities.

Dipole Moment Effect on the Memory Characteristics.

The electrical output and transfer characteristics of the devices are shown in Figures S6–S8 and Figure 4a–c. These output curves exhibit typical p-type field-effect transistor properties with the hole mobility of 0.014, 0.012, and 0.003 cm² V⁻¹ s⁻¹, respectively. The decrease of mobility when compared with the standard device (0.60 cm² V⁻¹ s⁻¹) may be attributed to the poor crystalline and small grain size of pentacene as revealed in Figure 3d–f. It should be noted that the programming voltage can be further reduced by reducing the thickness of tunneling

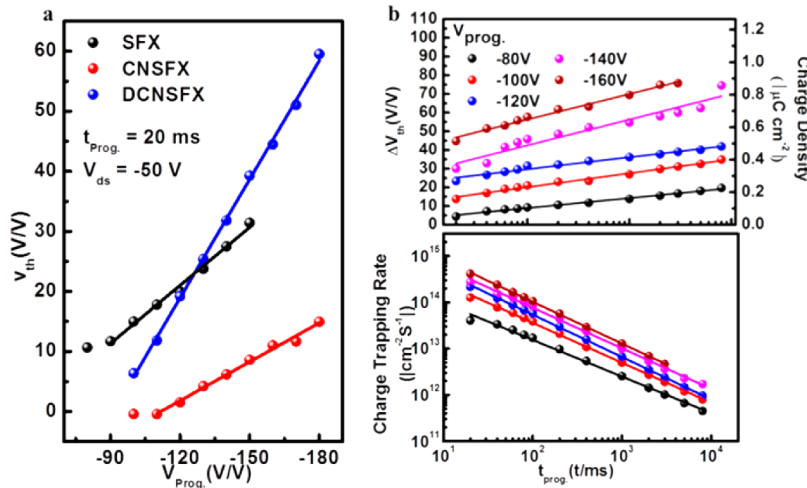


Figure 5. (a) Shifts of threshold voltage (ΔV_{th}) and linear fitting curves under different programming gate bias (V_{Prog}) with the negative bias. (b) ΔV_{th} , charge density, and charge trapping rate as the function of programming time (t_{Prog}) in the DCNSFX-based transistor.

dielectric layer. Figure 4a–c shows the typical shift in transfer curve of the transistor memory devices under electrical writing and photoerasing operation mode. We program the transistor memory devices at the same program conditions in the dark circumstance as the negative gate voltage (V_{Prog}) of -160 V and programming time (t_{Prog}) of 20 ms . All the devices are found to be repeatable in memory windows by examining different cells (~ 50 cells measured). The negative shifts of the transfer curves reveal typical hole trapping behaviors which indicate holes are injected from pentacene into SFXs. The DCNSFX and SFX exhibit a larger memory window as 39.3 and 31.4 V , compared with 8.6 V for CNSFX, respectively. Because of nearly the same charge density distribution between CNSFX and DCNSFX according to the ESP analysis (Figure 1d), the smaller dipole moment rather than the charge dispersion can be the reason for such easier hole tunneling from pentacene to SFX and DCNSFX film. A slightly larger memory window of DCNSFX vs SFX may attribute to its stronger hindrance effect by the bulky cyano substitution (discussed later). All the transistors exhibit stepwise negative shifts of transfer curve with the increase of the negative gate bias (Figures S9–S11). They indicate that these memory devices can process the multibit storage function to achieve high storage density in one cell. What we find interesting is that the positive programming in dark does not bring any change in transfer curves even $V_{Prog} = 180 \text{ V}$ and $t_{Prog} = 1 \text{ s}$ are applied. As is well-known, pentacene is a typical p-type semiconductor whose electron concentration is extremely low, especially in the air circumstance. Although the trapped electrons already located at the LUMO of pentacene, the electron tunneling through the triangle barrier is impossible without further charge accumulation at the interface due to no more electrons generate under the positive gate bias. Furthermore, electrons cannot be injected into pentacene from Au electrode either. Therefore, we speculate that the electrical nonerasing progress is owing to the unavailable neutralization of trapped holes in the HOMO of SFXs (Figure S12a) even in such high positive programming voltage. To this end, the electrical nonerasable memory devices in dark are constructed with SFXs, as the MCSEs, where a larger memory window can be obtained from SFXs with a weaker dipole moment.

It should be noted that all the programmed MCSEs-based transistor memories display a typical erasing process and

recover to the initial state after exposing the devices under light irradiation (with the power density of 1.8 mW cm^{-2} for 1 s), without any voltage operation. The mechanism of photoerasing progress is shown in Figure S12b. We deduce that the trapped holes at HOMO of SFXs may suffer typical charge-exciton annihilation at the SFXs/pentacene heterojunction with light exposure, which has been well investigated in photovoltaic devices.⁴¹ Pentacene is excited by the visible light, and the generated photoexciton is concentrated at the interface without remarkable charge separation (owing to the poor electron acceptance feature of SFXs). Thereby charge-exciton annihilation happens immediately as a result of neutralization of trapped holes in SFXs and electrons in pentacene.⁴² The operation method through photoirradiation rather than voltage provides not only a typical flash memory but also a smart strategy for information encryption as the feasible elimination of stored information.

The switching stabilities of the SFXs based devices are evaluated through write–read–erase–read (WRER) cycles, as shown in Figures S13–S15. The WRER cycles are operated through different conditions every $\sim 5 \text{ s}$ (all the drain currents are measured at $V_{ds} = -30 \text{ V}$), as follows subsequently: electrical writing in dark ($V_{Prog} = -160 \text{ V}$), reading ($V_g = -30 \text{ V}$ for SFX and DCNSFX, while -10 V for CNSFX), photoerasing (light power density 1.8 mW cm^{-2} , $V_g = 0 \text{ V}$), followed by another reading pulse. All the SFXs based transistor memory follows a repeatable WRER cycle. However, the on/off current ratios are only 10^1 – 10^2 during the reading steps. We test the retention properties of SFXs-based transistor memory to investigate their charge maintenance feature in dark. However, all the drain-source currents (I_{ds}) of ON state (without programming) are found to decrease dominantly, after $\sim 100 \text{ s}$ reading (Figure 4d and Figures S16, 17). It can be attributed to the continuous hole injection from Au drain-source electrode to pentacene finally to the SFXs layer by continuously adding reading pulse in negative V_{ds} without any additional blocking layer. Therefore, the polymer blocking layer is incorporated to further optimize the device configuration for the defecation of the dipole moment effect and long-term charge maintenance (discussed later).

Charge Storage Capacity Analysis. In order to further analyze how the dipole moment influences the hole trapping behavior, we plot the ΔV_{th} with programming gate voltage

(V_{Prog}) (Figure 5a) and programming time (t_{Prog}) (Figure 5b and Figures S18, S19) (ΔV_{th} are calculated from their transfer curves). All the devices display linear fittings in SFX, CNSFX, and DCNSFX based devices, corresponding to the model of Fowler–Nordheim (F–N) tunneling.⁵ The charge density (ρ) of trapping also takes the linear plot vs V_{Prog} and is estimated to be ca. 0.02–0.87 $\mu\text{C cm}^{-2}$. In the SFX-based FET, only \sim 13 V programming voltage is required. Such a rather low hole tunneling barrier at the pentacene/SFX heterojunction may arise from the aggregation in SFX film, leading to an unexpected excimer emission (Figure S5). The larger slope of DCNSFX indicates a stronger charge trapping capability than that of SFX and CNSFX at a higher $|V_{\text{Prog}}|$ region (>125 V). We suppose such extreme strong charge trapping ability is attributed to the hindrance effect of DCNSFX, as the HOMO located spiro plane is encapsulated by the symmetrical substituted cyano groups. However, in the case of lower $|V_{\text{Prog}}|$ (<125 V), it is well consisted with the lower dipole moment the larger ΔV_{th} , $\Delta V_{\text{th}}(\text{CNSFX}) < \Delta V_{\text{th}}(\text{DCNSFX}) < \Delta V_{\text{th}}(\text{SFX})$, indicating that the dipole moment dominates their trapping ability. The rather low capability of CNSFX further proves that a large dipole moment is unfavorable for the hole injection. As a critical parameter, we further explore the programming speeds through their charge trapping rates (as a function of $dN_{\text{trap}}/dt_{\text{Prog}} = (c_i/e)(dV_{\text{Prog}}/dt_{\text{Prog}})$) by plotting ΔV_{th} vs $\ln(t_{\text{Prog}})$ and N_{trap} vs $\ln(t_{\text{Prog}})$ (Figure 5b). We find that each plot of ΔV_{th} vs $\ln(t_{\text{Prog}})$ displays an approximately linear correlation for both devices when different V_{Prog} are applied. The charge trapping rates ($dN_{\text{trap}}/dt_{\text{Prog}}$) observed vary between 10^{14} – 10^{11} , 10^{13} – 10^{11} , and 10^{14} – 10^{11} $\text{cm}^{-2} \text{s}^{-1}$ for SFX, CNSFX, and DCNSFX, respectively (summarized in Table 2), with the pulse width

Table 2. Comparison of the Charge Density and Charge Trapping Rate of SFX, CNSFX, and DCNSFX

	charge density (cm^{-2})	charge trapping rate ($\text{cm}^{-2} \text{s}^{-1}$)
SFX	1.06×10^{13} – 1.79×10^{12}	1.73×10^{14} – 5.28×10^{11}
CNSFX	6.22×10^{12} – 3.88×10^{11}	7.85×10^{13} – 2.52×10^{11}
DCNSFX	1.39×10^{13} – 8.09×10^{11}	4.12×10^{14} – 4.52×10^{11}

(t_{Prog}) changing from 20 ms to 5 s in this process. Compared with polar CNSFX, a much higher charge trapping rate of DCNSFX and SFX suggests a smaller dipole moment in a symmetrical system which processes larger hole tunneling speeds. All the hole trapping speeds of SFXs-based MCSEs are significantly faster than those of metal-floating gate structure ($\sim 10^9 \text{ cm}^{-2} \text{s}^{-1}$).⁴³ It suggests that symmetrical SFXs with smaller dipole moment and larger hindrance are promising MCSEs toward high-density organic memory devices with a smart responsive feature.

Device Optimization. In order to exclude the morphology effects of the SFXs vapor films (Figure 3a–c) and obtain a better retention property, we blended SFXs into polystyrene (PS) for smooth thin-film MCSEs with pretty good mobility. The lower HOMO level of PS provides a deeper trapping site⁵ and avoids the charge escaping from the trapping layer (Figure 6a). We mix 10 wt % SFXs in polystyrene (PS) solution (5 mg/mL toluene) and spin-coat the solution at 3000 rpm for 30 s onto the substrate to construct the organic small molecular doping polymer dielectric layer which can trap high-density charge in the MCSEs. The output and transfer curves are shown in the Figures S20–S24 and Figure 6b. The drain-source currents of these optimized p-type transistors have been

enhanced dramatically, which can be attributed to favor pentacene growth in PS as well as a larger grain size of pentacene on PS top (Figures S25 and S26). As Figure S25 shows that the AFM topographic images of SFXs/PS are very smooth, whose rms values are 0.206, 0.350, and 0.194 nm respectively for SFX/PS, CNSFX/PS, and DCNSFX/PS. It means that we can exclude the morphology effect of the SFXs vapor films to investigate the dipole moment effect on hole storage for transistor memory. The higher drain-source currents of FET benefit a larger on/off ratio in MCSEs-based transistor memory devices. As expected, the SFXs in PS matrix also exhibit the same dipole moment effects on the memory windows, which are 41.7 and 48.0 V for SFX/PS- and DCNSFX/PS-based devices, respectively, much larger than that of CNSFX/PS (11.4 V). Without taking account of the morphology or defects of MCSEs layer, the SFXs molecules when mixed in PS solution exhibit their intrinsic trapping capability. Therefore, it proves that the design of a weak dipole moment of MCSEs in favor of high-performance transistor memory with high charge density. Furthermore, all the memory characteristics have also been slightly enhanced when the doping MCSEs with PS strategy is applied, thereafter the photoerasing process is also observed. The WRER cycles in SFXs/PS-based devices are evaluated as shown in Figure 6c and Figures S27 and S28. As the lower concentration of SFXs in PS, the photoerasing takes longer time. Therefore, the positive gate bias ($V_{\text{Prog}} = 120$ V) is incorporated to accelerate the erasing process, in this case. Similar to previous discussion, devices based on SFXs/PS MCSEs exhibit excellent stability but possess much higher on/off current ratios (10^3 – 10^4) in WRER cycles. Fortunately, we find pretty good retention properties whose I_{ds} can maintain over 10^4 s, integrating with a high on/off ratio, nearly 10^4 , at a reading gate voltage of -10 V (Figure 6d and Figures S29, S30). Therefore, such excellent retention properties of transistor memory devices suggest that the approach of doping MCSEs with a short dipole moment into polymer offers a feasible way to fabricate organic nonvolatile memories for high density information storage with controllable charge behaviors.

CONCLUSIONS

In summary, we have designed and synthesized a series of cyano-substituted SFXs serving as molecular charge storage elements (MCSEs) to investigate the dipole moment effects on charge trapping behaviors. The dipole moments of SFXs are ordered as μ_{SFX} (0.9956 D) $<$ μ_{DCNSFX} (1.5925 D) \ll μ_{CNSFX} (5.5110 D), without changing their HOMO level. The prototype transistor memory based on SFXs exhibits an erasable type feature with smart photoresponsive feature. The weaker dipole moments of SFX and DCNSFX, rather than the stronger that of CNSFX, exhibit excellent hole trap ability as larger memory windows (30–40 V) and trapping density ($\sim 1 \times 10^{13} \text{ cm}^{-2}$). The optimized devices with SFXs blended in polystyrene further confirm such dipole moment effects to get rid of their film morphology effects to obtain better retention property. Therefore, bulky D-A-type symmetrical molecule with a weak dipole moment has been proved as an effective molecular design principle of MCSEs for high performance transistor memory. Such dipole moment effect of small molecular MCSEs will guide scientists to uncover not only the memory mechanism of OFET memory but also the smart information encryption in future data storage according to their photoresponse feature.

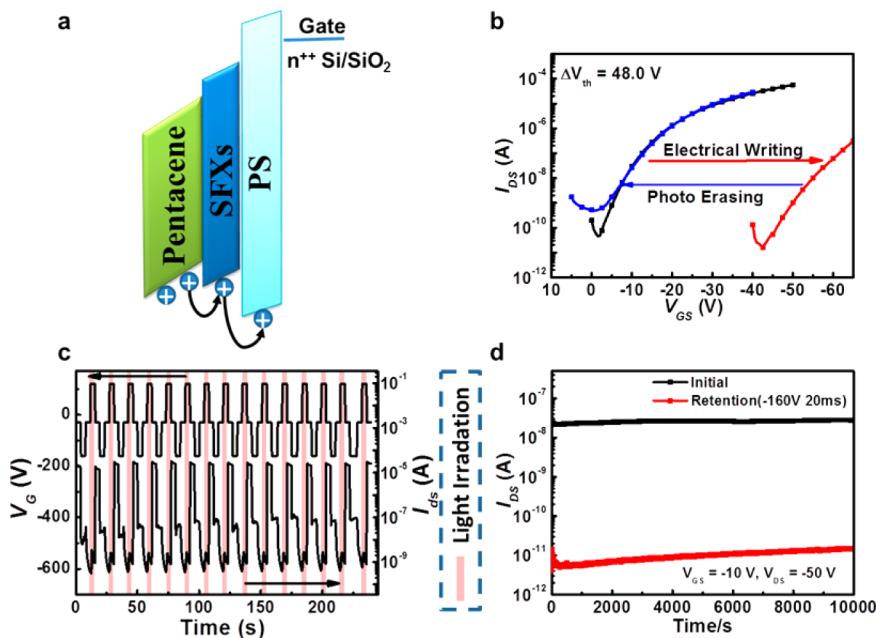


Figure 6. (a) Energy level diagrams of the SFXs blended in PS. (b) Reversible shifts in V_{th} and the transfer characteristic of the transistor before and after gate bias in dark with DCNSFX blended in PS. The drain current was measured at $V_{ds} = -50 \text{ V}$. The programming bias (V_{Prog}) was -160 V , and programming time (t_{Prog}) was 20 ms . (c) Reversible current response to the WRER cycles of DCNSFX blended with PS based transistors. The currents at ON and OFF states were read at $V_g = -30 \text{ V}$ and $V_d = -30 \text{ V}$. (d) Retention test of DCNSFX blended in PS-based transistor.

ASSOCIATED CONTENT

Supporting Information

Measurement details of NMR, CV, UV-PL spectra, AFM images. The Supporting Information is available free of charge on the ACS Publications website at DOI: [10.1021/acs.jpcc.5b03867](https://doi.org/10.1021/acs.jpcc.5b03867).

AUTHOR INFORMATION

Corresponding Authors

*E-mail [iamlhixie@njupt.edu.cn](mailto:iamlhxie@njupt.edu.cn) (L.H.X.).

*E-mail iammdyi@njupt.edu.cn (M.D.Y.).

*E-mail wei-huang@njtech.edu.cn (W.H.).

Author Contributions

C.S. and Z.Q.L. contributed equally to this work.

Notes

The authors declare no competing financial interest.

ACKNOWLEDGMENTS

We express our sincere gratitude to the National Natural Science Funds for Excellent Young Scholar (21322402), National Natural Science Foundation of China (U1301243, 21373114, 21274064, 21144004, 60876010, 61177029, 20974046, 61136003), Open Project from State Key Laboratory of Supramolecular Structure and Materials at Jilin University (sklssm2015022), Doctoral Fund of Ministry of Education of China (20133223110007), Excellent science and technology innovation team of Jiangsu Higher Education Institutions (2013), Synergetic Innovation Center for Organic Electronics and Information Displays, Natural Science Foundation of Jiangsu Province, China (BK2008053, SJ209003, BM2012010). The project was funded by the Priority Academic Program Development of Jiangsu Higher Education Institutions, PAPD (YX03001).

REFERENCES

- Möller, S.; Perlov, C.; Jackson, W.; Taussig, C.; Forrest, S. R. A Polymer/Semiconductor Write-Once Read-Many-Times Memory. *Nature* **2003**, *426*, 166–169.
- Gelinck, G. H.; Huitema, H. E. A.; Van Veenendaal, E.; Cantatore, E.; Schrijnemakers, L.; Van der Putten, J.; Geuns, T. C. T.; Beenakkers, M.; Giesbers, J. B.; Huisman, B. H.; et al. Flexible Active-Matrix Displays and Shift Registers Based On Solution-Processed Organic Transistors. *Nat. Mater.* **2004**, *3*, 106–110.
- Xie, L. H.; Yin, C. R.; Lai, W. Y.; Fan, Q. L.; Huang, W. Polyfluorene-Based Semiconductors Combined With Various Periodic Table Elements for Organic Electronics. *Prog. Polym. Sci.* **2012**, *37*, 1192–1264.
- Xie, L. H.; Ling, Q. D.; Hou, X. Y.; Huang, W. An Effective Friedel-Crafts Postfunctionalization of Poly(N-Vinylcarbazole) to Tune Carrier Transportation of Supramolecular Organic Semiconductors Based on π -Stacked Polymers for Nonvolatile Flash Memory Cell. *J. Am. Chem. Soc.* **2008**, *130*, 2120–2121.
- Guo, Y. L.; Di, C. A.; Ye, S. H.; Sun, X. N.; Zheng, J.; Wen, Y. G.; Wu, W. P.; Yu, G.; Liu, Y. Q. Multibit Storage of Organic Thin-Film Field-Effect Transistors. *Adv. Mater.* **2009**, *21*, 1954–1959.
- Führer, M. S.; Kim, B. M.; Durkop, T.; Brintlinger, T. High-Mobility Nanotube Transistor Memory. *Nano Lett.* **2002**, *2*, 755–759.
- Orgiu, E.; Crivillers, N.; Herder, M.; Grubert, L.; Pätzelt, M.; Frisch, J.; Pavlica, E.; Duong, D. T.; Bratina, G.; Salleo, A.; et al. Optically Switchable Transistor via Energy-Level Phototuning in a Bicomponent Organic Semiconductor. *Nat. Chem.* **2012**, *4*, 675–679.
- Chou, Y. H.; Takasugi, S.; Goseki, R.; Ishizone, T.; Chen, W. C. Nonvolatile Organic Field-Effect Transistor Memory Devices Using Polymer Electrets with Different Thiophene Chain Lengths. *Polym. Chem.* **2014**, *5*, 1063–1071.
- Di, C. A.; Zhang, F. J.; Zhu, D. B. Multi-Functional Integration of Organic Field-Effect Transistors (OFETs): Advances and Perspectives. *Adv. Mater.* **2013**, *25*, 313–330.
- Sekitani, T.; Yokota, T.; Zschieschang, U.; Klauk, H.; Bauer, S.; Takeuchi, K.; Takamiya, M.; Sakurai, T.; Someya, T. Organic Nonvolatile Memory Transistors for Flexible Sensor Arrays. *Science* **2009**, *326*, 1516–1519.

- (11) Ahmed, R.; Kadashchuk, A.; Simbrunner, C.; Schwabegger, G.; Havlicek, M.; Glowackic, E.; Sariciftci, N. S.; Baig, M. A.; Sitter, H. Photosensitivity of Top Gate C_{60} Based OFETs: Potential Applications for High Efficiency Organic Photodetector. *Org. Electron.* **2014**, *15*, 175–181.
- (12) Shin, I. S.; Kim, J. M.; Jeun, J. H.; Yoo, S. H.; Ge, Z.; Hong, J. I.; Ho Bang, J.; Kim, Y. S. Nonvolatile Floating Gate Organic Memory Device Based on Pentacene/CdSe Quantum Dot Heterojunction. *Appl. Phys. Lett.* **2012**, *100*, 183307/1–4.
- (13) Baeg, K. J.; Noh, Y. Y.; Sirringhaus, H.; Kim, D. Y. Controllable Shifts in Threshold Voltage of Top-Gate Polymer Field-Effect Transistors for Applications in Organic Nano Floating Gate Memory. *Adv. Funct. Mater.* **2010**, *20*, 224–230.
- (14) Du, Z. Z.; Li, W.; Ai, W.; Tai, Q.; Xie, L. H.; Cao, Y.; Liu, J. Q.; Yi, M. D.; Ling, H. F.; Li, Z. H.; et al. Chemoselective Reduction of Graphene Oxide and Its Application in Nonvolatile Organic Transistor Memory Devices. *RSC Adv.* **2013**, *3*, 25788–25791.
- (15) Kang, M.; Baeg, K. J.; Khim, D.; Noh, Y. Y.; Kim, D. Y. Printed, Flexible, Organic Nano-Floating-Gate Memory: Effects of Metal Nanoparticles and Blocking Dielectrics on Memory Characteristics. *Adv. Funct. Mater.* **2013**, *23*, 3503–3512.
- (16) Zhang, L.; Wu, T.; Guo, Y. L.; Zhao, Y.; Sun, X. N.; Wen, Y. G.; Yu, G.; Liu, Y. Q. Large-Area, Flexible Imaging Arrays Constructed by Light-Charge Organic Memories. *Sci. Rep.* **2013**, *3*, 1080/1–9.
- (17) Saragi, T. P. I.; Spehr, T.; Siebert, A.; Fuhrmann-Lieker, T.; Salbeck, J. Spiro Compounds for Organic Optoelectronics. *Chem. Rev.* **2007**, *107*, 1011–1065.
- (18) Jung, M. H.; Song, K. H.; Ko, K. C.; Lee, J. Y.; Lee, H. Nonvolatile Memory Organic Field Effect Transistor Induced by the Steric Hindrance Effects of Organic Molecules. *J. Mater. Chem.* **2010**, *20*, 8016–8020.
- (19) Shih, C. C.; Chiu, Y. C.; Lee, W. Y.; Chen, J. Y.; Chen, W. C. Conjugated Polymer Nanoparticles as Nano Floating Gate Electrets for High Performance Nonvolatile Organic Transistor Memory Devices. *Adv. Funct. Mater.* **2015**, *25*, 1511–1519.
- (20) Chiu, Y. C.; Otsuka, I.; Halila, S.; Borsali, R.; Chen, W. C. High-Performance Nonvolatile Transistor Memories of Pentacene Using the Green Electrets of Sugar-Based Block Copolymers and Their Supramolecules. *Adv. Funct. Mater.* **2014**, *24*, 4240–4249.
- (21) Ling, Q. D.; Liaw, D. J.; Teo, E. Y. H.; Zhu, C.; Chan, D. S. H.; Kang, E. T.; Neoh, K. G. Polymer Memories: Bistable Electrical Switching and Device Performance. *Polymer* **2007**, *48*, 5182–5201.
- (22) Bringezu, F.; Brezesinski, G.; Mohwald, H. Influence of Side-Chain Length on Phospholipid Ordering in Two Dimensions. *Chem. Phys. Lipids* **1998**, *94*, 251–260.
- (23) Baxendale, I. R.; Ley, S. V. Polymer-Supported Reagents for Multi-Step Organic Synthesis: Application to the Synthesis of Sildenafil. *Bioorg. Med. Chem. Lett.* **2000**, *10*, 1983–1986.
- (24) Pay davosi, S.; Aidala, K. E.; Brown, P. R.; Hashemi, P.; Supran, G. J.; Osedach, T. P.; Hoyt, J. L.; Bulovic, V. Detection of Charge Storage on Molecular Thin Films of Tris(8-hydroxyquinoline) Aluminum (Alq_3) by Kelvin Force Microscopy: A Candidate System for High Storage Capacity Memory Cells. *Nano Lett.* **2012**, *12*, 1260–1264.
- (25) Pay davosi, S.; Abdu, H.; Supran, G. J.; Bulovic, V. Performance Comparison of Different Organic Molecular Floating-Gate Memories. *IEEE Trans. Nanotechnol.* **2011**, *10*, 594–599.
- (26) Zhou, Y.; Han, S. T.; Sonar, P.; Roy, V. A. L. Nonvolatile Multilevel Data Storage Memory Device from Controlled Ambipolar Charge Trapping Mechanism. *Sci. Rep.* **2013**, *3*, 2319/1–7.
- (27) Wu, W. P.; Zhang, H. L.; Wang, Y.; Ye, S. H.; Guo, Y. L.; Di, C. G.; Yu, G.; Zhu, D. B.; Liu, Y. Q. High-Performance Organic Transistor Memory Elements with Steep Flanks of Hysteresis. *Adv. Funct. Mater.* **2008**, *18*, 2593–2601.
- (28) Baeg, K. J.; Khim, D.; Kim, D. Y.; Jung, S. W.; Koo, J. B.; Noh, Y. Y. Organic Nano-Floating-Gate Memory with Polymer:[6, 6]-Phenyl- C_{61} Butyric Acid Methyl Ester Composite Films. *Jpn. J. Appl. Phys.* **2010**, *49*, 05EB01/1–5.
- (29) Baeg, K.-J.; Noh, Y.-Y.; Ghim, J.; Lim, B.; Kim, D.-Y. Polarity Effects of Polymer Gate Electrets on Non-Volatile Organic Field-Effect Transistor Memory. *Adv. Funct. Mater.* **2008**, *18*, 3678–3685.
- (30) Osikowicz, W.; de Jong, M. P.; Salaneck, W. R. Formation of the Interfacial Dipole at Organic-Organic Interfaces: C_{60} /Polymer Interfaces. *Adv. Mater.* **2007**, *19*, 4213–4217.
- (31) Oh, D. H.; Sano, M.; Boxer, S. G. Electroabsorption (Stark-Effect) Spectroscopy of Monoruthenium and Biruthenium Charge-Transfer Complexes-Measurements of Changes in Dipole-Moments and Other Electrooptic Properties. *J. Am. Chem. Soc.* **1991**, *113*, 6880–6890.
- (32) Chiu, Y. C.; Chen, T. Y.; Chueh, C. C.; Chang, H. Y.; Sugiyama, K.; Sheng, Y. J.; Hirao, A.; Chen, W. C. High Performance Nonvolatile Transistor Memories of Pentacene Using the Electrets of Star-Branched p-Type Polymers and Their Donor-Acceptor Blends. *J. Mater. Chem. C* **2014**, *2*, 1436–1446.
- (33) Lin, J. Y.; Li, W.; Yu, Z. Z.; Yi, M. D.; Ling, H. F.; Xie, L. H.; Li, S. B.; Huang, W. π -Conjugation-Interrupted Hyperbranched Polymer Electrets for Organic Nonvolatile Transistor Memory Devices. *J. Mater. Chem. C* **2014**, *2*, 3738–3743.
- (34) Chiu, Y. C.; Liu, C. L.; Lee, W. Y.; Chen, Y.; Kakuchi, T.; Chen, W. C. Multilevel Nonvolatile Transistor Memories Using a Star-Shaped Poly((4-diphenylamino)benzyl methacrylate) Gate Electret. *NPG Asia Mater.* **2013**, *5*, e35/1–7.
- (35) Qian, Y.; Xie, G. H.; Chen, S. F.; Liu, Z. D.; Ni, Y. R.; Zhou, X. H.; Xie, L. H.; Liang, J.; Zhao, Y. Z.; Yi, M. D.; et al. A New Spiro Fluorene-9,9'-Xanthene-Based Host Material Possessing no Conventional Hole- and Electron-Transporting Units for Efficient and Low Voltage Blue PHOLED via Simple Two-Step Synthesis. *Org. Electron.* **2012**, *13*, 2741–2746.
- (36) Baeg, K. J.; Binda, M.; Natali, D.; Caironi, M.; Noh, Y. Y. Organic Light Detectors: Photodiodes and Phototransistors. *Adv. Mater.* **2013**, *25*, 4267–4295.
- (37) Xie, L. H.; Liu, F.; Tang, C.; Hou, X. Y.; Hua, Y. R.; Fan, Q. L.; Huang, W. Unexpected One-Pot Method to Synthesize Spiro Fluorene-9,9'-Xanthene Building Blocks for Blue-Light-Emitting Materials. *Org. Lett.* **2006**, *8*, 2787–2790.
- (38) Xie, L. H.; Liang, J.; Song, J.; Yin, C. R.; Huang, W. Spirocyclic Aromatic Hydrocarbons (SAHs) and Their Synthetic Methodologies. *Curr. Org. Chem.* **2010**, *14* (18), 2169–2195.
- (39) Weissman, S. A.; Zewge, D.; Chen, C. Ligand-Free Palladium-Catalyzed Cyanation of Aryl Halides. *J. Org. Chem.* **2005**, *70*, 1508–1510.
- (40) Han, S. T.; Zhou, Y.; Xu, Z. X.; Roy, V. A. L.; Hung, T. F. Nanoparticle Size Dependent Threshold Voltage Shifts in Organic Memory Transistors. *J. Mater. Chem.* **2011**, *21*, 14575–14580.
- (41) Hodgkiss, J. M.; Albert-Seifried, S.; Rao, A.; Barker, A. J.; Campbell, A. R.; Marsh, R. A.; Friend, R. H. Exciton-Charge Annihilation in Organic Semiconductor Films. *Adv. Funct. Mater.* **2012**, *22*, 1567–1577.
- (42) Yi, M. D.; Xie, M.; Shao, Y. Q.; Li, W.; Ling, H. F.; Xie, L. H.; Yang, T.; Fan, Q. L.; Zhu, J. L.; Huang, W. Light Programmable/Erasable Organic Field-Effect Transistor Ambipolar Memory Devices Based on the Pentacene/PVK Active Layer. *J. Mater. Chem. C* **2015**, *3*, 5220–5225.
- (43) Kolodny, A.; Nieh, S. T. K.; Eitan, B.; Shappir, J. Analysis and Modeling of Floating-Gate EEPROM Cells. *IEEE Trans. Electron Devices* **1986**, *33*, 835–844.